Response to RC1

The article is well-structured, and the technique and results are thoroughly explained. However, there are a few important comments:

Reply:

Thank you for your positive assessment and thoughtful comments. Our responses to each point are provided below.

1. At what depths was in-situ data used to confirm soil freezing beyond 5 cm? Freezing to a depth of 5 cm is a significant criterion for some agricultural activities, but it is insufficient for the majority of hydrological and ecological tasks, particularly in the context of climate change.

Reply:

Thank you for your inquiry regarding the depth of in situ measurements used for validating soil freezing. In validating both the coarse-resolution and high-resolution freeze-thaw (FT) datasets, we exclusively relied on ground-based soil temperature data from depths shallower than 5 cm. The initial coarse-resolution FT discrimination is derived from AMSR-E/2 passive-microwave brightness temperatures (TBs) at K-band (18.7 GHz) and Ka-band (36.5 GHz), whose typical penetration depths are approximately 3–5 cm and 0–2 cm, respectively, both under 5 cm. Given these penetration-depth constraints of passive microwave sensing, we confined our validation to shallow (<5 cm) observations to ensure that the in situ data and satellite-derived classifications sample the same sensitive soil layer. We also acknowledge the importance of deeper FT dynamics for climate and ecosystem studies and may investigate remote-sensing approaches for monitoring and analyzing greater freeze depths in future work.

We have revised Sections 2.5 and 4.4.2 to clearly state the depths of ground-based soil temperature measurements used for validation and to explain the rationale for focusing on shallow (<5 cm) layers.

Changes in manuscript:

Lines 177-178 in Section 2.5:

"This study selected long-term in situ soil temperature data from 1,027 stations within 44 global networks, all measured at a depth of 0–5 cm to match the penetration depth of the passive microwave observations."

Lines 518-520, 525-527 in Section 4.4.2:

"Additionally, the utilization of 0–5 cm depth data ensures comparability with satellite-based FT

discrimination, since the typical penetration depths of passive microwave observations at 18.7 GHz and 36.5 GHz are approximately 3–5 cm and 0–2 cm, respectively, both under 5 cm."

"However, the use of 0–5 cm soil temperature remains the most physically meaningful for passive microwave FT validation, as it provides a more direct and reliable indicator of the near-surface state than either air temperature or deeper soil temperature measurements."

2. How do the authors incorporate data on permafrost distribution into the FT product, both in extended areas and mountainous regions? How do authors account for geographical and temporal variations in permafrost indicators between 2002 and 2023?

Reply:

Thank you for your question. We address it in two parts:

First, **we did not incorporate any existing permafrost-distribution maps into our FT dataset.** As shown in Fig. 1, we only used three IGBP land-cover classes as masking layers: water bodies, urban and built-up lands, and snow and ice. No permanent-permafrost map was employed, either in the extended areas or in mountainous regions. This explanation has been added to Section 2.4 of the revised manuscript.

Second, although our 0.05° FT dataset focuses on near-surface soil phase transitions, it enables the derivation of annual FT metrics (e.g. the number of frost days, the number of FT cycles) for each grid cell. Mapping these metrics across diverse landscapes provides a remote sensing approach to assess spatial and temporal variations in permafrost extent from 2002 to 2023.

For instance, **while our dataset does not use any existing permafrost distribution data as input,** the results show spatial agreement between the annual number of frost days derived from our remote sensing approach in 2017 and independently derived permafrost maps over the Qinghai–Tibetan Plateau (Zhao, 2017), as illustrated in Fig. 8 of the revised manuscript. Specifically, the average annual frost days within permafrost-classified pixels is approximately 278.85, indicating a potential spatial correspondence between these two metrics. This qualitative comparison demonstrates that **regions with high annual numbers of frost days, as detected by remote sensing, are generally consistent with areas classified as permafrost in existing reference datasets**, supporting the potential of the annual number of frost days to serve as a valuable proxy for assessing permafrost extent and its spatial variability. This discussion has been added at the end of Section 4.3.1 of the revised manuscript.

Changes in manuscript:

Lines 165-168 in Section 2.4:

“The land cover dataset, illustrated in Fig. 1, was specifically utilized to mask out pixels of three IGBP land-cover classes: water bodies, urban and built-up lands, and snow and ice. Furthermore, the corresponding type percentage dataset was used to filter out pixels dominated by large water bodies, which were then explicitly marked in the FT data record. Notably, no permafrost distribution data were used as input or constraints in generating the FT dataset.”

Lines 457–465, Figure 8 in Section 4.3.1:

“To further explore the climatic and geocryological significance of this metric, we compared the spatial distribution of annual frost days in 2017 with independently derived permafrost maps over the Qinghai–Tibetan Plateau (Zhao, 2017; Zou et al., 2017), as illustrated in Fig. 8. This qualitative comparison reveals a notable spatial agreement, demonstrating that regions with high annual numbers of frost days, as detected by remote sensing, are generally consistent with areas classified as permafrost in existing reference datasets. Specifically, the average annual frost days within permafrost-classified pixels is approximately 278.85, indicating a potential spatial correspondence between these two metrics. This finding highlights the potential of the annual number of frost days as a valuable proxy for assessing permafrost extent and its spatial variability.”

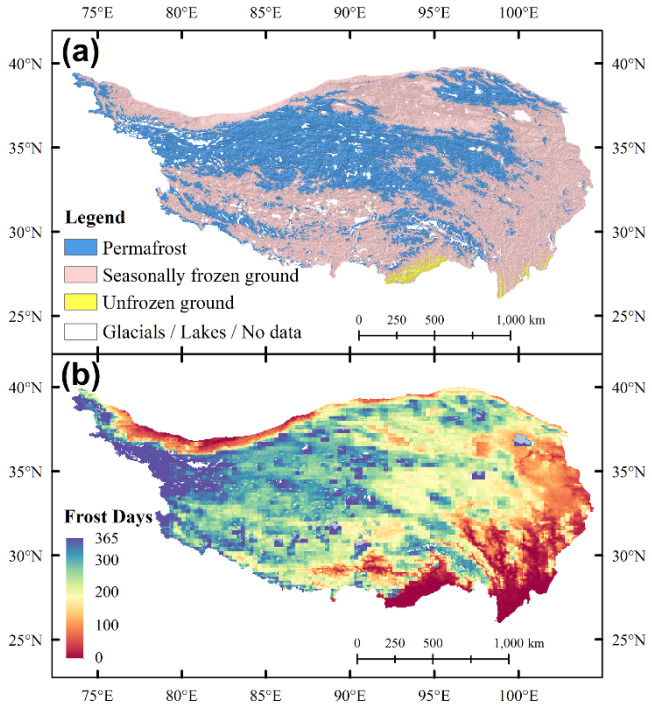

Figure 8: Maps of (a) permafrost distribution map (Zhao, 2017), and (b) annual frost days derived from the downscaled descending FT product in 2017 over the Qinghai–Tibet Plateau.

Lines 799–800, 820-822 in Reference:

Zhao, L.: A new map of permafrost distribution on the Tibetan Plateau (2017), National Tibetan Plateau /

Third Pole Environment Data Center [dataset], https://doi.org/10.11888/Geocry.tpdc.270468, 2017.

Zou, D., Zhao, L., Sheng, Y., Chen, J., Hu, G., Wu, T., Wu, J., Xie, C., Wu, X., Pang, Q., Wang, W., Du, E., Li, W., Liu, G., Li, J., Qin, Y., Qiao, Y., Wang, Z., Shi, J., and Cheng, G.: A new map of permafrost distribution on the tibetan plateau, The Cryosphere, 11, 2527–2542, https://doi.org/10.5194/tc-11-2527-2017, 2017.

3 The authors do not provide a convincing number of point verifications of the FT product in various physiographic conditions using statistical techniques. In addition, a comparison of soil freezing depth inaccuracies in various natural zones is required.

Reply:

Thank you for your valuable suggestion.

To address the issue of insufficient point verifications across different physiographic conditions and land cover types, we have added a statistical accuracy table based on the ESA CCI Land Cover 2010 classifications provided by ISMN sites (see Table 4 of the revised manuscript and Response Fig. 1). This table presents classification accuracies of both coarse-resolution (0.25°) and high-resolution (0.05°) products across different land cover types, with separate statistics for ascending and descending satellite passes, thereby reflecting the accuracy under various physiographic conditions and land cover types. This content has been included in Section 4.2 of the revised manuscript.

As for the comparison of soil freezing depth inaccuracies across natural zones, we are initiating a follow-up study that uses the annual total frozen-days metric from our FT dataset to simulate soil freezing depths and assess their variability across different natural regions. A detailed comparison will be presented in future work.

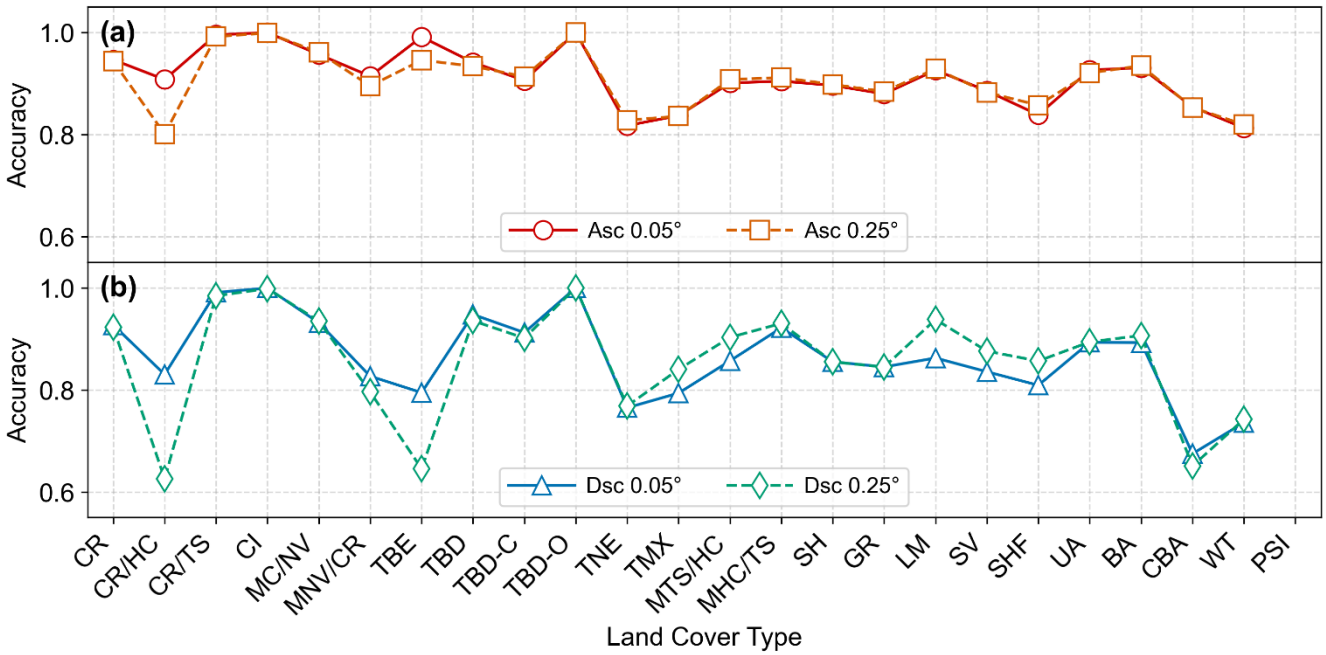

Response Figure 1: Line plots of classification accuracy for the 0.25° and 0.05° FT products across different land cover types: (a) ascending passes; (b) descending passes. The x-axis abbreviations are explained in Response Table 1

Response Table 1: ESA CCI land cover classification framework.

Code	ESA CCI Land Cover Classes		Code	ESA CCI Land Cover Classes	
	Abbreviated name	Full name		Abbreviated name	Full name
10	CR	Cropland, rainfed	100	MTS/HC	Mosaic tree and shrub (>50%) / herbaceous cover (<50%)
11	CR/HC	Cropland, rainfed / Herbaceous cover	110	MHC/TS	Mosaic herbaceous cover (>50%) / tree and shrub (<50%)
12	CR/TS	Cropland, rainfed / Tree or shrub cover	120	SH	Shrubland
20	CI	Cropland, irrigated or post-flooding	130	GR	Grassland
30	MC/NV	Mosaic cropland (>50%) / natural vegetation (tree, shrub, herbaceous cover) (<50%)	140	LM	Lichens and mosses
40	MNV/CR	Mosaic natural vegetation (tree, shrub, herbaceous cover) (>50%) / cropland (<50%)	150	SV	Sparse vegetation (tree, shrub, herbaceous cover) (<15%)
50	TBE	Tree cover, broadleaved, evergreen, Closed to open (>15%)	180	SHF	Shrub or herbaceous cover, flooded, fresh/saline/brakish water
60	TBD	Tree cover, broadleaved, deciduous,	190	UA	Urban areas

		Closed to open (>15%)			
61	TBD-C	Tree cover, broadleaved, deciduous, Closed (>40%)	200	BA	Bare areas
62	TBD-O	Tree cover, broadleaved, deciduous, Open (15-40%)	201	CBA	Consolidated bare areas
70	TNE	Tree cover, needleleaved, evergreen, closed to open (>15%)	210	WT	Water
90	TMX	Tree cover, mixed leaf type (broadleaved and needleleaved)	220	PSI	Permanent snow and ice

Changes in manuscript:

Lines 412-415 in Section 4.2:

In addition, Table 4 summarizes the classification accuracies of both products across various land cover types for both ascending and descending passes. The land cover types are defined by the ESA CCI Land Cover 2010 classification values provided by the ISMN sites, enabling a more comprehensive assessment of performance under different physiographic conditions.

Lines 430-432, Table 4 in Section 4.2:

Table 4 Validation results for the coarse- and high-resolution FT products across various land cover types. Land cover types are sourced from the ESA CCI Land Cover 2010 classification values provided within the ISMN site dataset.

No	Land cover type	Ascend			Descend		
		Num	Accuracy (0.05°)	Accuracy (0.25°)	Num	Accuracy (0.05°)	Accuracy (0.25°)
1	Cropland, rainfed	275,743	94.66%	94.37%	277,149	92.71%	92.26%
2	Cropland, rainfed / Herbaceous cover	10,129	90.79%	80.11%	10,157	83.01%	62.56%
3	Cropland, rainfed / Tree or shrub cover	12,127	99.54%	99.20%	11,336	99.07%	98.42%
4	Cropland, irrigated or post-flooding	5,162	99.99%	99.91%	5,217	99.93%	99.81%
5	Mosaic cropland (>50%) / natural vegetation (tree, shrub, herbaceous cover) (<50%)	4,896	95.70%	96.12%	5,439	93.14%	93.47%
6	Mosaic natural vegetation (tree, shrub, herbaceous cover) (>50%) / cropland (<50%)	25,702	91.44%	89.54%	27,613	82.67%	79.58%
7	Tree cover, broadleaved,	7,466	99.14%	94.58%	12,210	79.45%	64.53%

	evergreen, Closed to open (>15%)						
8	Tree cover, broadleaved, deciduous, Closed to open (>15%)	12,658	94.14%	93.40%	12,094	94.76%	93.53%
9	Tree cover, broadleaved, deciduous, Closed (>40%)	15,445	90.60%	91.34%	14,557	91.21%	90.13%
10	Tree cover, broadleaved, deciduous, Open (15-40%)	198	100.00%	100.00%	198	100.00%	100.00%
11	Tree cover, needleleaved, evergreen, closed to open (>15%)	898,729	81.77%	82.81%	996,959	76.49%	76.84%
12	Tree cover, mixed leaf type (broadleaved and needleleaved)	10,529	83.71%	83.61%	12,351	79.36%	84.00%
13	Mosaic tree and shrub (>50%) / herbaceous cover (<50%)	22,384	90.10%	90.79%	24,002	85.67%	90.28%
14	Mosaic herbaceous cover (>50%) / tree and shrub (<50%)	5,159	90.48%	91.17%	4,955	92.15%	93.02%
15	Shrubland	217,565	89.63%	89.83%	236,376	85.49%	85.47%
16	Grassland	596,806	87.98%	88.41%	626,309	84.49%	84.47%
17	Lichens and mosses	2,711	92.62%	92.88%	3,153	86.24%	93.78%
18	Sparse vegetation (tree, shrub, herbaceous cover) (<15%)	25,240	88.56%	88.26%	28,065	83.54%	87.57%
19	Shrub or herbaceous cover, flooded, fresh/saline/brakish water	16,913	83.87%	85.76%	19,753	80.89%	85.64%
20	Urban areas	41,406	92.64%	92.07%	37,230	89.29%	89.39%
21	Bare areas	2,955	93.10%	93.49%	3,178	89.26%	90.64%
22	Consolidated bare areas	642	85.41%	85.31%	665	67.48%	65.08%
23	Water	5,213	81.31%	81.96%	6,120	73.57%	74.23%
24	Permanent snow and ice	0	/	/	0	/	/

4. Can you explain the lack of freeze-thaw data at 0.25° resolution in Fig. 4?

Reply:

Thank you for this question.

The lack of 0.25° freeze-thaw (FT) data shown in Fig. 4(a) and (b) arises from the satellite's inherent

orbital swath gaps in daily AMSR-E/2 passive-microwave brightness-temperature (TB) observations. Because each overpass only covers a limited swath, grid cells outside that swath on any given day lack valid TB inputs, making FT discrimination at 0.25° impossible and resulting in missing values. The approximately 2-day revisit interval of AMSR-E/2 causes the location of valid observations to shift from one day to the next. Although this results in missing measurements for certain pixels on some dates, each pixel still accumulates sufficient valid observations over the course of a year.

In contrast, Fig. 4(c) and (d) show our 0.05° high-resolution downscaled product, which contains no data gaps because our pixel-by-pixel linear-regression downscaling automatically skips any dates with missing inputs. Specifically, for each 0.25° pixel, regression fitting was performed using only those dates with valid 0.25° FT data, together with the corresponding 0.05° optical data on those dates. The 0.05° optical data are spatiotemporally continuous, so regression fitting is always possible on any date with valid 0.25° FT observations. For example, if a given pixel has valid 0.25° FT data on only 200 out of 365 days, the regression coefficients are derived solely from those 200 days. We then apply the fitted model to the full year of 0.05° optical data, thereby generating a seamless 0.05° FT dataset.

A detailed description of this linear-regression downscaling approach and how it addresses missing data is provided in Section 3.3 of the manuscript. Additionally, Section 4.1 provides a brief description of the data gaps present in the 0.25° product, while highlighting that the 0.05° downscaled product contains no such gaps.

Changes in manuscript:

Lines 259, 267, 270-272 in Section 3.3:

"where the coefficients a, b and c are determined through linear regression fitting."

"Linear regression fitting was performed on these three data vectors of each pixel, resulting in six coefficient matrices for a, b, and c at the ascending and descending times:"

"where the abbreviations "HR" and "LR" refer to high and low resolution, respectively. Regression fitting was performed using only those dates with valid 0.25° FT data, together with the corresponding 0.05° optical data on those dates."

Lines 361-363, 370-378 in Section 4.1:

"The left panel of Fig. 4 presents a comparison between the original 0.25° FT discrimination product and the downscaled FT discrimination product for January 1, 2019, at 01:30 (descending orbit)."

"In addition to the classification of surface conditions, another important feature of the dataset is its treatment of missing data. In the original 0.25° FT product, data gaps occur due to the inherent swath gaps

of the AMSR-E/2 satellites, resulting in missing values for some grid cells on certain days. By contrast, our downscaling approach for the 0.05° product effectively overcomes this limitation. For each 0.25° pixel, regression fitting is performed using only those dates with valid 0.25° FT data, together with the corresponding 0.05° optical data on those dates. As the 0.05° optical data are spatiotemporally continuous, regression can always be performed on any date with valid 0.25° FT observations. The fitted regression model is then applied to the complete year of 0.05° optical data, resulting in a seamless, gap-free 0.05° FT dataset. This missing-data treatment in the downscaling process ensures that the high-resolution FT product contains no data gaps, as demonstrated in Fig. 4.”